Seismic stability of steel wide-flange columns in ductile moment-resisting frames: out-of-plane response and design recommendations

Abrar Islam[1] · Ali Imanpour[2]

Abstract

This paper examines the seismic stability of steel wide-flange columns located in the first storey of Ductile Moment-Resisting Frames (MRFs) with emphasis on their out-of-plane response and proposes improved stability design recommendations for such columns. A five-storey steel MRF is first designed in accordance with the seismic provisions of the Canadian steel design standard. A subassembly consisting of the exterior bay plus half of the adjacent interior bay is then isolated from the prototype MRF, and its finite element model is constructed. The results obtained from the nonlinear response history analysis of the MRF subassembly is used to assess the stability response of the first-storey columns and verify the adequacy of a component-based column model, which is isolated from the MRF, in predicting column nonlinear cyclic response. A total of 26 seismically-compact wide-flange columns covering a wide range of geometrical parameters, including global slenderness, cross-section aspect and section width-to-thickness ratios, are subjected to cyclic strong-axis displacement and weak-axis bending in the presence of a constant axial compression load. The results of the column parametric study are used to identify column out-of-plane instability modes using strength and deformation response parameters, including base moment, axial shortening, out-of-plane displacement, and cross-section twist. Two instability modes, including out-of-plane buckling at the base and member buckling, are observed. A design equation as a function of parameters affecting the out-of-plane stability of columns with base plastic hinging, namely global slenderness, cross-section aspect and axial load ratios, is finally proposed to verify the out-of-plane stability of first-storey columns under seismic loading.

Keywords Steel moment-resisting frames · Wide-flange columns · Out-of-plane stability response · Seismic design · Nonlinear simulation

---

Extended author information available on the last page of the article

1 Introduction

Steel moment-resisting frames (MRFs) are considered as a desirable seismic force-resisting system for the construction of building structures in high seismic areas due to their high architectural versatility, relatively long-span beams and significant ductility capacity. Type D (Ductile) steel MRF system is the most ductile frame system in the 2019 Canadian steel design standard, CSA S16 (CSA 2019). Flexural plastic hinging at beam ends and column bases is the anticipated nonlinear mechanism in multi-storey Ductile MRFs. Beams and columns in this system are designed to carry the combination of gravity and seismic loads, satisfy the strong column-weak beam criterion at every beam-to-column joint, and meet code-specified inter-storey drift limits. The latter often dominates member selection in Ductile MRFs. Similar provisions can be found in other design standards such as the U.S. Seismic Provisions for Steel Buildings AISC 341 (AISC 2016a), New Zealand steel design standard NZS 3404 (NZS 1997) and Eurocode 8 (EN1998-1 2003).

In the North American construction practice, columns of low-to-mid-rise steel MRFs often consist of wide-flange members resisting lateral seismic load by bending about their strong-axis. First-storey fixed-base columns with anticipated base plastic hinging are expected to possess sufficient strength and remain stable when the beams reach their probable flexural resistances. Furthermore, these columns along with upper-storey columns and beams should have sufficient flexural stiffness to ensure that frame inter-storey drifts do not exceed the drift limit specified by the respective building code, e.g., 2.5% per the National Building Code, NBC, of Canada (NRC 2015). Columns with deep wide-flange sections (i.e., $d/b_f \geq 1.7$, where d is the overall depth of the cross-section and b_f is the flange width) are therefore ideal in MRF design since they offer higher lateral stiffness and moment capacity compared to square wide-flange sections (i.e., $d/b_f \approx 1.0$) with the same weight.

A set of uncoupled seismic design checks are prescribed by CSA S16 for the first-storey columns with anticipated base plastic hinging in Ductile (Type D) MRFs to ensure ductile and stable behaviour under major seismic events. The width-to-thickness ratios of such columns shall comply with the limits corresponding to Class 1 sections (or highly compact members in AISC Seismic Provisions) that are $b_f/2t_f = 7.8$ and $h/t_w = 55$ for the flange and web, respectively, where b_f, t_f, h and t_w are the flange width, flange thickness, web clear depth and web thickness, respectively. The web width-to-thickness limits was computed assuming a factored axial load of $C_f = 0.15AF_y$ where A is the cross-sectional area and F_y is the yield strength of the material conforming to ASTM A992 Gr. 50 steel with $F_y = 345$ MPa, which shall be taken as 350 MPa when verifying width-to-thickness ratios. For out-of-plane stability or lateral bracing check, the unbraced length of the first-storey column L_b (i.e., storey height) shall be limited to $r_y (17{,}250 + 15500\kappa)/F_y$ where r_y is the radius of gyration of the column section about its weak-axis and the factor κ is the ratio of the smaller to the larger factored end moments, which is positive for double curvature and negative for single curvature. This factor represents the distribution of bending along the length of the member and leads to a more liberal lateral bracing limit when it is positive. κ shall be set equal to zero in lieu of a rational analysis, which would give a global slenderness ratio, L_b/r_y, limit of 50 assuming Fy = 345 MPa, eliminating the majority of deep wide-flange profiles that can otherwise be ideal to meet the stringent storey drift limit. Islam and Imanpour (2022) recommended $\kappa = 0.45$ when verifying column lateral bracing, which would result in L_b/r_y limit of 70. CSA S16 also requires that the factored axial load of the first-storey columns of Type D

MRFs be limited to $0.30AF_y$ when the frame is located in high seismic regions. This limit is intended to avoid the rapid degradation of the flexural strength of the member under high axial loads, which can limit column ductility under seismic loading (CISC 2021). Finally, for the columns subjected to a factored axial load greater than or equal to $0.15AF_y$, a more stringent limit for the web width-to-thickness ratio $h/t_w \leq 700/(F_y)^{0.5}$ compared to that of Class 1 sections shall be met. CSA S16 requires that in-plane and lateral-torsional buckling stability be verified for all the columns except the first–storey column under combined axial force and bending, which may affect the selection of the first-storey column as the same W-shape profile is typically used in the first and second stories. Despite detailed stability requirements provided by CSA S16, these requirements, namely the lateral bracing check and axial load limits, lack sufficient background research and may, in some cases, lead to conservative designs. This conservatism, e.g., increase in steel tonnage, has been demonstrated in Islam and Imanpour (2022) for steel MRFs designed including such requirements as compared to those designed when the CSA S16 stability requirements are relaxed.

More comprehensive special seismic design requirements compared to those specified in CSA S16 exist in the NZS 3404 standard for first storey fixed-base steel MRF columns, which is mostly based on the findings by MacRae et al. (1990). These columns should have Full Lateral Restraint (FLR) to ensure that they can develop their full plastic flexural strength over the storey height, i.e., a stability verification when the column moment reaches its plastic moment capacity. Moreover, full lateral restraint shall be provided to both column flanges within the yielding region length, which is defined as the length over which the flexural bending demand exceeds 0.75 to 0.85 times the member flexural resistance. Finally, three axial force limits are prescribed by NZS 3404 (Brownlee 1994). The first limit is intended to limit the axial compression force to ensure that the member can deliver the expected inelastic demand. The second limit, known as the End Yielding Criteria (EYC), aims to prevent the moment at any point over the column length from exceeding the base moment. The third limit relates to the gravity-induced axial force, which is intended to delay local buckling and minimize column axial shortening (Penga et al. 2008).

Unlike CSA S16, EC8 (EN1998-1 2003) explicitly requires that stability of the first-storey column with base plastic hinging be verified using axial force-bending moment interaction equations for in-plane and out-of-plane buckling limit states under the loading scenario at which beams and column base reach their respective plastic moment resistances. This stability requirement in EC8 is analogous to the FLR criterion in NZS 3404.

The inelastic cyclic behaviour of wide-flange columns and beam-to-column moment connections in steel MRFs was the focus of a large number of research studies in the past (Popov et al. 1975; Nakashima et al. 1990; MacRae et al. 1990; Popov et al. 1998; Yu et al. 2001; FEMA 355D 2000; Shen et al. 2002; Zhang and Ricles 2006; Newell and Uang 2008). The experimental study by Newell and Uang (2008) involved the investigation of the cyclic response of wide-flange columns isolated from steel buckling-restrained braced frames under varying axial load and lateral displacement histories. These columns had nearly square cross-sections ($d/b_f \approx 1.0$) with low width-to-thickness ratios, i.e., Class 1 flange and web. It was shown that square wide-flange columns remain stable under even high axial compression loads and can offer significant rotational capacity without significant degradation in flexural strength or large twist. Over the past decade, the focus of steel wide-flange column research has shifted to the cyclic response of columns with deep cross-sections ($d/b_f \geq 1.7$) as those profiles are more commonly used in the construction of MRF

buildings. Full-scale experimental testing performed in Canada (Elkady and Lignos 2014, 2017, 2018a; Cravero et al. 2020) and the U.S. (Ozkula et al. 2017a, b, 2021; Uang et al. 2019) along with high-fidelity numerical simulations (Ozkula et al. 2017b, Elkady and Lignos 2018b) performed on specimens representing the fixed-base columns of multi-storey steel MRFs confirmed that local buckling at the end plastic hinge locations typically controls the flexural capacity of deep wide-flange columns at large drift ratios. It was also found that column cyclic response is a function of its end conditions. For instance, the columns having a fixed-flexible end condition experienced less severe local buckling at their flexible end, suggesting a more realistic end condition should be considered in the performance evaluation of such columns. Furthermore, the columns with large global slenderness ratios ($L_b/r_y \geq 80$) may be prone to out-of-plane instability, including weak-axis flexural buckling or lateral-torsional buckling, at large storey drifts. Despite significant advancement of knowledge in understanding the nonlinear cyclic response of steel wide-flange columns, the effect of the limit states observed in the past studies on member stability response has not yet been quantified taking into account the influence of out-of-plane bending demands under a more representative loading scheme (e.g., earthquake ground motions). Furthermore, seismic design recommendations in the framework of the Canadian design practice that account for the combined effects of the parameters affecting the stability condition of fixed-base wide-flange columns are required.

This paper aims to first evaluate the stability response of wide-flange columns located in the first-storey of steel MRFs under seismic loading with the focus on out-of-plane response and second propose enhanced stability design recommendations for such columns. A prototype five-storey Ductile MRF is first designed in accordance with CSA S16 seismic provisions. The continuum-based finite element model (CFEM) of the selected MRF's subassembly consisting of the exterior bay plus a half of the adjacent interior bay is then created. The results from the Nonlinear Response History Analysis (NLRHA) of the subassembly model are used to examine the stability response of the frame with emphasis on the interior first-storey column and measure out-of-plane bending anticipated under seismic loading. A parametric study of 26 isolated first-storey interior columns covering a wide range of L_b/r_y, d/b_f, b/t_f and h/t_w under cyclic strong-axis displacement and weak-axis bending histories in the presence of a constant axial compression load is completed. The parametric study results are finally used to interrogate the parameters affecting the seismic stability of wide-flange columns located in the first storey of Ductile steel MRFs and propose stability design recommendations for such columns.

2 Building selected and loading

A five-storey office building located on site class C in Vancouver, British Columbia, Canada (a high seismic region in Canada) was selected to evaluate seismic stability of steel MRFs. The plan view of the building along with live, dead and snow loads are shown in Fig. 1a. The dimensions of the building in the plan are 52.5×37.5 m. The height of the first storey is 4.3 m, and the upper stories are 4.0 m-tall. Continuous columns are used over the first and second stories, with a splice at Storey 3 joining them to columns covering the rest of the building height. One of the perimeter frames in the long direction, as shown in Fig. 1a, was selected and designed as a Ductile (Type D) steel MRF.
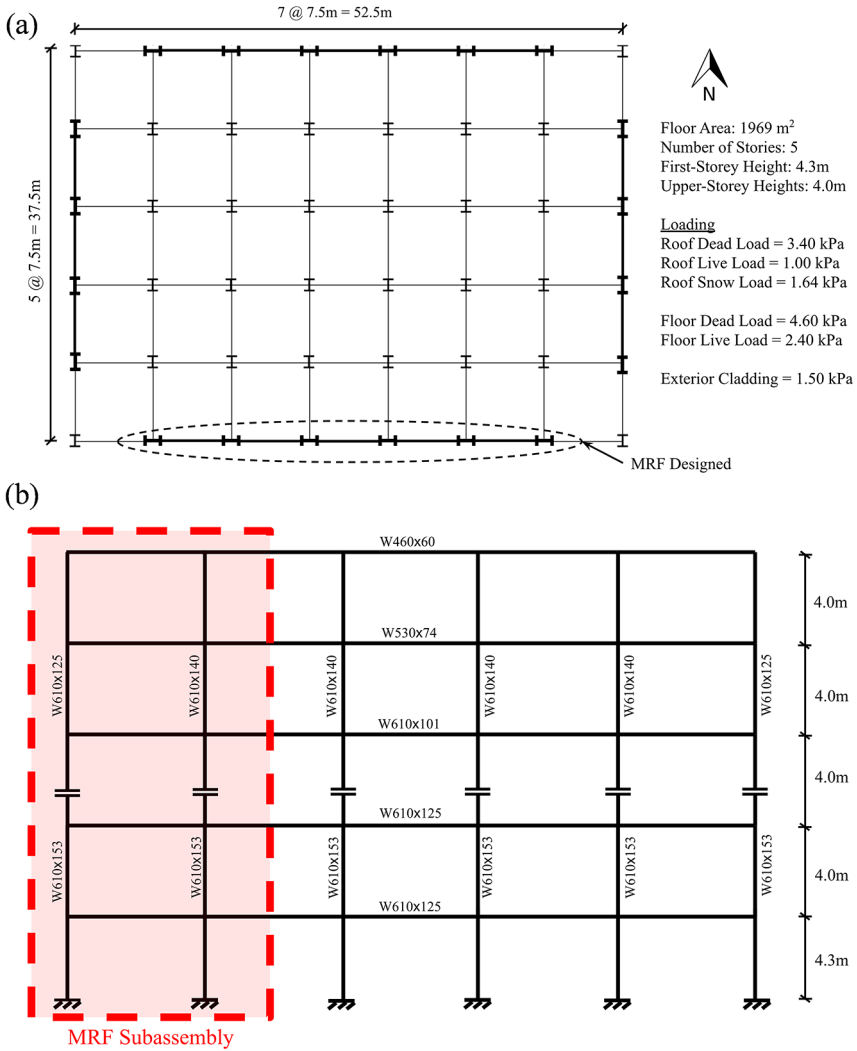
Fig. 1 Five-storey office building: (**a**) Plan view; (**b**) MRF elevation and selected member sizes

Loading was performed in accordance with the 2015 NBC. In the calculation of gravity loads, it was assumed that the secondary beams (steel open web joists) run in the North-South direction (Fig. 1) and deliver gravity loads to the beams of the MRF considered here. The seismic base shear for the preliminary design was calculated using the equivalent static force procedure. The building is of normal importance with the seismic importance factor $I_E = 1.0$. The higher mode factor M_v is taken as 1.0. The overstrength- and ductility-related force modification factors are $R_o = 1.5$ and $R_d = 5.0$, respectively. The design period, i.e., the minimum of the fundamental period obtained from a modal analysis and 1.5 times the period computed using the empirical equation, is $T_a = 1.22$s, resulting in a design spectral

acceleration of 0.388 g. The seismic weight tributary to the selected MRF is $W = 22,347$ kN. A modal response spectrum analysis was also performed taking into account the effects of accidental torsion, notional load, and P-Delta effects to achieve a more realistic seismic force distribution and lateral frame deflections.

3 Member design

The MRF was designed following CSA S16-19 using wide-flange (W-shape) beams and columns conforming to ASTM A992 Gr. 50 steel with a minimum specified yield strength $F_y = 345$ MPa and probable yield strength $R_y F_y = 385$ MPa. Beam-to-column moment connections consist of reduced beam section (RBS) connections designed in accordance with the CISC Moment Connections for Seismic Applications (CISC 2014) assuming that limited shear yielding can develop in the column panel zone.

The design of the MRF was an iterative process where the strength requirements and the drift limit were verified in each iteration. The beams were first designed as a flexural member under gravity plus seismic load effects, while their sections were adjusted subsequently to meet the storey drift limit and RBS connection requirements. Within each design iteration, the strong column-weak beam ratio at each beam-to-column joint, in-plane and out-of-plane stability of the columns in Stories 2–5 were verified. Storey drifts were then checked against the 2.5% limit considering the effects of reduced stiffness due to RBS through a 10% amplification applied to the elastic drift of the structure (CISC 2014). Figure 1b shows the selected member sizes for the MRF. The member design was mainly governed by the drift check performed using a longer design period $T_a = 1.79$s computed as the minimum of the analytical period from a modal analysis and an upper bound limit of 2.0 s.

A W610×153 column with $b/t_f = 4.6$, $h/t_w = 40.9$, $d/b_f \approx 2.7$ and $L_b/r_y \approx 85.0$ was selected for the interior and exterior first-storey columns. The global slenderness ratio of the W610×153 column exceeds the lateral bracing limit (=50 with $\kappa = 0$ and $F_y = 345$ MPa). Moreover, it possesses a web width-to-thickness ratio of 40.9, above the limit of 37 specified for columns with base plastic hinging under an axial compression load equal to or exceeding $0.15AF_y$. Based on the MRF design, the interior first-storey column was subjected to an axial compression load of just $0.15AF_y$, while the exterior first-storey column was subjected to a maximum axial compression load above $0.30AF_y$. However, this selection was intended to critically evaluate the current section and global slenderness ratio limits for first-storey columns of Ductile steel MRFs (Imanpour et al. 2016). Moreover, past studies have shown that both limits may be conservative for exterior columns, which heavily benefit from largely fluctuating axial loads due to dynamic overturning effects (Islam and Imanpour 2022).

4 MRF stability response

4.1 Continuum-based finite element model

An MRF subassembly consisting of the exterior bay plus half of the adjacent interior bay was selected as shown in Fig. 1b. A three-dimensional Continuum-based Finite Element

Model (CFEM) of the MRF subassembly was developed in the ABAQUS program (Simulia 2020). This model was intended to study the seismic stability response of steel MRFs when subjected to ground motion accelerations taking into account the stiffness of the adjoining beams and columns, the influence of exterior column uplift, and out-of-plane bending demands arising from RBS connections. Furthermore, the subassembly model can aid in better understanding of the seismic stability response of deep slender ($L_b/r_y > 50$) wide-flange columns and in developing stability design requirements.

The beams and columns of the MRF were simulated using four-node doubly curved, reduced integration, hourglass controlled Shell elements (S4R). The mesh size was varied across the model to optimize the computation time without sacrificing accuracy. A 25×25 mm mesh was used for the first-storey columns, at column web panel zones and RBSs where yielding is expected. A coarse mesh was employed in locations where yielding or instability is not expected, e.g., an element size of 25×75 mm was used between the column panel zones in upper-storey columns and outside RBS locations. The RBS connection was constructed explicitly by trimming flanges to create the RBS circular cut. Doubler plates in the column panel zones were simulated when required by increasing the thickness of elements in the column web between beam flanges. Continuity plates were provided in the column web at the level of the top and bottom flanges of the beams.

The steel material was defined using Young's modulus, $E = 200$ GPa, Poisson's ratio $\upsilon = 0.3$, and the expected yield stress $R_y F_y = 385$ MPa. Material nonlinearity was incorporated in the model through the Maxwell-Huber-Hencky-von Mises yield criterion with associated flow rule. The nonlinear cyclic behaviour of the steel material was reproduced using the Voce-Chaboche plasticity model that features combined isotropic/kinematic hardening (de Castro e Sousa et al. 2020; Hartloper et al. 2021; Elkady and Lignos 2018b) using the kinematic hardening parameters, $C = 3378$ MPa and $\gamma = 20$, and cyclic hardening parameters, $Q_\infty = 90$ MPa and $b = 12$. To trigger local instability in the columns, initial geometric out-of-straightness was created in the web and flanges at their both ends within each storey. Maximum amplitudes of initial imperfections were set equal to $b_f/150$ and $d/150$ in the flange and web, respectively, which correspond to maximum anticipated manufacturing errors of wide-flange profiles (ASTM 2003). For both beams and columns, global out-of-plane out-of-straightness was created following the elastic buckling mode shape of the respective member with a maximum amplitude of 0.001 times the unsupported length of the member (AISC 2016b). The modeling assumptions were verified by comparing the cyclic behaviour of an isolated wide-flange column against the experimental test data reported by Elkady and Lignos (2018a). Refer to Islam and Imanpour (2022) for further information on the numerical model.

Figure 2 shows the boundary conditions considered to simulate the MRF subassembly. All translational and rotational DOFs were restrained at the base of the column, except the translational DOF along Z-axis (in the plane of the frame) to allow for horizontal movement resulting from base excitation created by the ground motion acceleration. At the top end of the column of each storey at the level of the beam top flange, the translational and rotational DOF of the column nodes were coupled to a reference point (RP) located at the middle of the column web (Fig. 2b). The out-of-plane translational DOF in X-axis was restrained at this RP to represent the lateral support provided by the perpendicular beams framing into columns at the storey level. The concrete slab was not explicitly modeled as it would crack at large storey drifts as observed in past experimental studies (Ricles et al. 2004). The
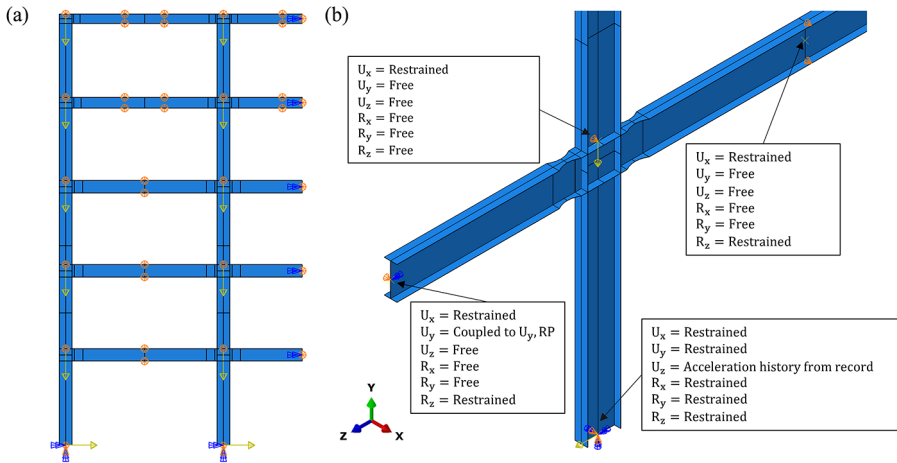
Fig. 2 Subassembly model and boundary conditions: (**a**) Elevation view; (**b**) first-storey interior column (elements are not shown)

translational DOF of the top end of both interior and exterior columns at each storey (at RPs) were coupled in Z-axis to avoid relative horizontal displacements between columns. Out-of-plane bracing for the beams was provided at beam mid-span at both top and bottom flanges (Fig. 2a), which was simulated by restraining translation in X-axis at the exterior beam mid-span and the free end of the beam of the interior bay. No bracing was provided at RBS locations as per the exception by AISC Prequalified Connections (2016c) for beam lateral bracing in the presence of concrete slab to create more critical out-of-plane demands on the first-storey column.

The axial gravity load tributary to each column at each storey was applied at the respective column RP. A leaning column, consisting of rigid beam-column wire elements, was created to account for P-Delta effects. The rotational DOFs of the leaning column were released at the two ends within each storey. Moreover, the translational DOF of the leaning column was coupled to that of the MRF subassembly at each storey using a kinematic coupling constraint. Rayleigh damping corresponding to 2% of critical was used to reproduce classical damping. The corresponding mass and stiffness proportional damping coefficients were assigned based on the structure's first and second modes of vibration obtained from a vibration analysis performed on the subassembly model. The subassembly model was analyzed using the implicit dynamic analysis method under the ground motion acceleration applied to the base in Z-axis.

A set of 33 earthquake ground motions consisted of three potential seismicity sources in Vancouver, i.e., crustal, deep in-slab, and subduction interface (11 records per each scenario). The ground motions were scaled to match on average the NBC design response spectrum representing a hazard level with 2% probability of exceedance in 50 years (NRC-Commentaries 2015; Tremblay et al. 2015). The concentrated plasticity-based model of the prototype MRF (Fig. 1b) developed in the OpenSEES program (Mckenna et al. 1997) as described in Islam and Imanpour (2022), which requires a significantly lower computational cost to perform the NLRHA compared to the subassembly CFEM, was used to perform the NLRHA under the 33 ground motion records and to select three most critical records
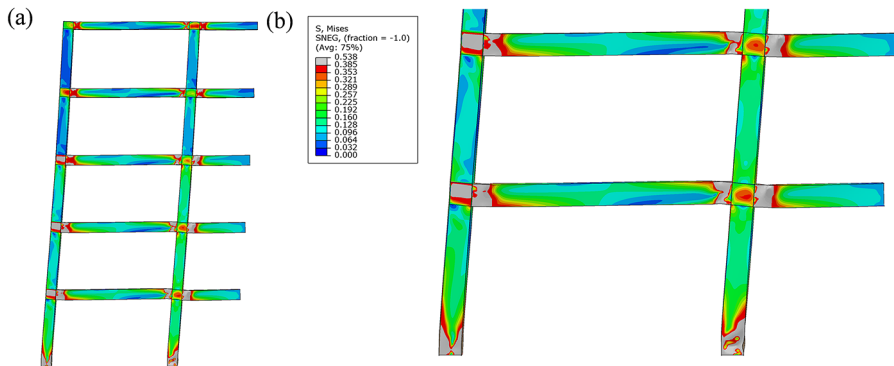
Fig. 3 Deformed-shape and von Mises stress distributions at $t=156$s under the 2011 Tohoku, Japan -YMT002 earthquake: (**a**) Elevation view; (**b**) Storey 1 and 2 (gray area represents yielding)

that produced the three largest deformation demands in Storey 1 of the prototype MRF. These records, including 2007 Pisco, Peru – UNICA, 2010 Maule, Chile – SSA2, and 2011 Tohoku, Japan – YMT002, were then used to perform the NLRHA using the subassembly CFEM. Refer to Islam (2022) for the details of the selected ground motions and the NLRHA using the concentrated plasticity-based model of the MRF. The key CFEM analysis results, including nonlinear mechanism, behaviour of first-storey beams and columns, under the 2011 Tohoku, Japan – YMT002 earthquake, which is a subduction interface record, were presented in the following sub-sections. Past studies on steel MRFs also confirmed that subduction interface earthquakes are expected to create the largest drift demands in mid-rise MRF structures located in Vancouver (Mokhtari et al. 2022).

4.2 Overall response

Deformed-shape and von Mises stress distribution of the MRF subassembly at maximum storey drift ratio recorded in Storey 1, 3.4%, at $t=156$s is shown in Fig. 3a. At this point, the exterior column was in tension. A magnified view of Stories 1 and 2 shown in Fig. 3b confirms plastic hinging at the base of both columns along with significant yielding in RBS regions and shear yielding in column panel zones. Flexural plastic hinges first formed at the RBS regions of the first two stories and base of the first storey columns at $t=36$ s and then propagated to the upper storey beams and column panel zones. After beam plastic hinging when drift reached its maximum value, 3.4%, relatively large out-of-plane displacements occurred at RBS reduced zones (in the order of $1.3r_{yb}$ at $t=156$s where r_{yb} is the radius of gyration of the beam section about its weak-axis), compared to out-of-plane displacements observed earlier in the ground motion. These out-of-plane displacements were particularly more pronounced at the bottom two stories leading to twisting of first-storey columns (Chi and Uang 2002).
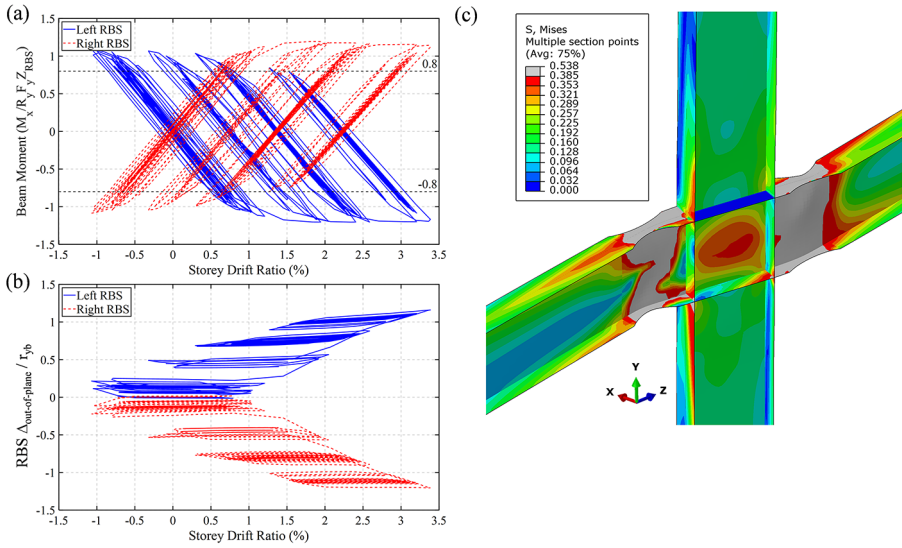
Fig. 4 Response of W610×125 beams adjoining the interior first-storey column under the 2011 Tohoku, Japan – YMT002 earthquake: (**a**) Moment – storey drift ratio; (**b**) Out-of-plane displacement at RBS normalized to weak-axis radius of gyration of the beam; (**c**) Connection deformed-shape at $t = 156$s, storey drift ratio 3.4% (gray area represents yielding)

4.3 Beam response

The strong-axis bending moments and out-of-plane displacements at the RBS location of the W610×125 beams adjoining the interior first-storey column are shown in Fig. 4a and b. The out-of-plane displacement at each RBS was computed by taking an average of the amplitudes recorded at the top and bottom of the web. In Fig. 4a and b, the left and right RBS (see Fig. 4c) and their displacement sign along X-axis are denoted based on the coordinate system shown in Fig. 4c.

As shown in Fig. 4a, beam moment reached a maximum value of $1.20 R_y F_y Z_{RBS}$ at 1.5% drift ratio and then reduced to $1.09 R_y F_y Z_{RBS}$ at 3.4% drift ratio at the right beam due to local buckling and out-of-plane movement in the RBS. In Fig. 4b, an increasing trend was observed for the out-of-plane displacement at RBS locations, while the rate of this increase tends to reduce at large drift ratios. The maximum out-of-plane displacement recorded was $1.3 r_{yb}$ for both beams connected to the column on each side but moving in opposite directions (left RBS moving along positive X-axis and right RBS moving along negative X-axis) as shown in Fig. 4c. This response caused twisting of the first-storey column. Furthermore, RBS displacements were slightly different (approximately $0.20 r_{yb}$) between the top and bottom of their respective cross-sections, generating twist in the beam due to non-uniform yielding of the top and bottom flanges in the presence of initial out-of-plane imperfections. The out-of-plane RBS response confirms the tendency of steel beams to buckle in the inelastic range with pronounced deformations in plastic hinge regions (Chi and Uang 2002). It should be noted that the cross-section twist and RBS out-of-plane displacement observed for the interior column was mainly produced because of the lack of supplemental
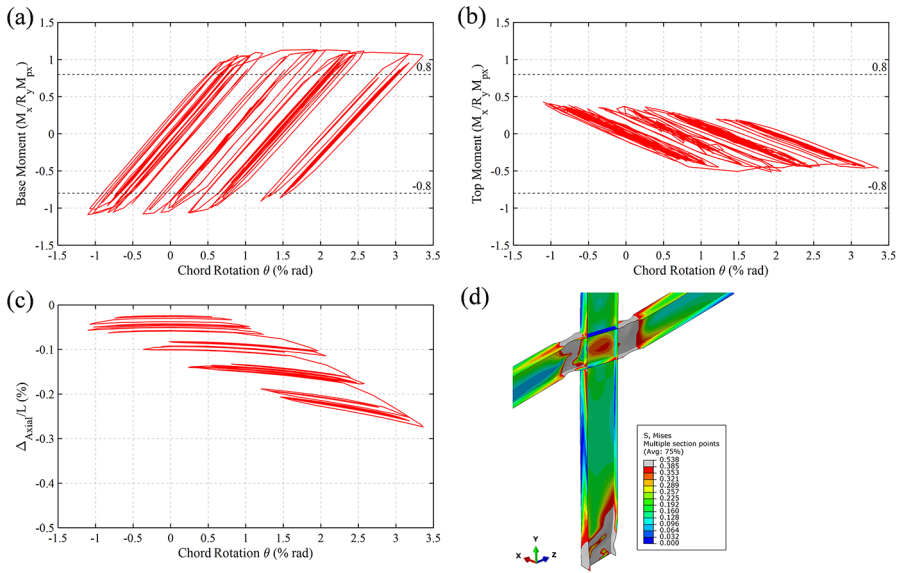
Fig. 5 In-plane response of the interior first-storey W610×153 column under the 2011 Tohoku, Japan – YMT002 earthquake: (**a**) Strong-axis moment vs. chord rotation at the base; (**b**) Strong-axis moment vs. chord rotation at the top end; (**c**) Axial shortening vs. chord rotation; (**d**) Deformed-shape and von Mises stress distribution at $t=156$s, chord rotation 3.4% (gray area represents yielding)

bracing at the RBS locations and could have significantly been reduced had lateral support been provided.

4.4 Column response

Moment-chord rotation responses at the base and top end of the interior first-storey W610×153 column is shown in Fig. 5a and b. Referring to Fig. 5a, the column experienced moderate strength degradation at its base, with the moment capacity reaching $1.05R_yM_{px}$ at 3.4% chord rotation from a maximum value of $1.13R_yM_{px}$ measured at 1.5% chord rotation. The loss of strength occurred mainly due to web and flange local buckling initiated at around 1.5% chord rotation and was exacerbated at higher drifts. Local buckling was accompanied by moderate axial shortening in the member under a constant axial load equal to $0.15AF_y$, which reached a maximum of 0.27%L as shown in Fig. 5c. The top moment, which was recorded right below the column panel zone, never exceeded $0.52R_yM_{px}$ (Fig. 5b), indicating no yielding at the column top end and an inflection point above column mid-height. The column deformed-shape and von Mises stress distribution at $t=156$s corresponding to 3.4% chord rotation is shown in Fig. 5d. In this figure, the minimal stress recorded at the top continuity plate is attributed to the kinematic coupling constraint assigned to the reference point to uniformly distribute the gravity loads throughout the column cross-section at the floor level.

Figure 6 shows the out-of-plane response of the first-storey interior column, including weak-axis moment demand, normalized out-of-plane displacement $\Delta_{\text{Out-of-Plane}}/L$ and normalized cross-section twist $\gamma_{\text{Cross-Section}}$ where L is the column clear length. The out-of-plane
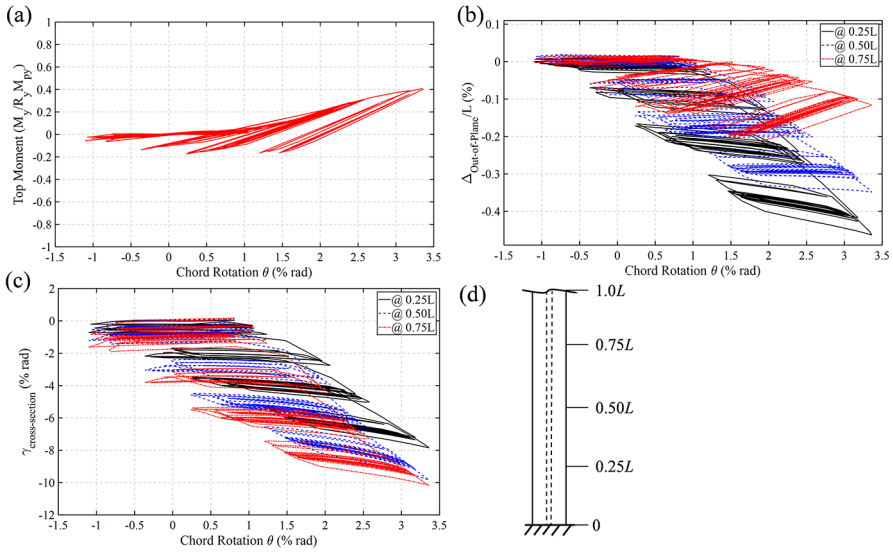
Fig. 6 Out-of-plane response of the interior first-storey W610×153mn under the 2011 Tohoku, Japan – YMT002 earthquake: (**a**) Weak-axis moment vs. chord rotation at the top; (**b**) Out-of-plane displacement vs. chord rotation; (**c**) Cross-section twist vs. chord rotation; (**d**) Recording stations along column length

deformation of the RBS plus that of the base plastic hinge due to local buckling near the base caused weak-axis moment at the top end of the column, which reached a maximum of $0.40R_yM_{py}$ as shown in Fig. 6a. The out-of-plane displacement and cross-section twist at quarter points, 0.25 L, 0.50 L, 0.75 L, with respect to the column length measured from the fixed base, is shown in Fig. 6b and c. To eliminate the effects of cross-section twist, the out-of-plane displacements were calculated by taking the average of the out-of-plane displacements at two extremes of the column web.

Out-of-plane displacement of the column (Fig. 6b) was more pronounced near the base of the column, i.e., 0.25 L, where local instability took place, reaching a maximum value of 0.46%L at 0.25 L, while lower peaks of 0.35%L and 0.21%L were recorded at 0.50 and 0.75 L, respectively. A reversed trend was observed for the cross-section twist (Fig. 6c) increasing toward the member's top-end where the twist is unrestrained. The cross-section twist at 0.75 L was recorded as 0.102 rad. (6.0 degrees) at 3.4% chord rotation. However, a lower peak twist angle was observed at 0.25 and 0.50 L, 0.078 and 0.098 rad., respectively, because of the higher fixity provided by the column base compared to the flexible top. The large twist angle (>0.10 rad.) observed here suggests that slender sections such as W610×153 may be prone to out-of-plane instability under earthquake loading.

The exterior first-storey W610×153 column experienced a large axial compression force ($0.32AF_y$) and a considerable tension force ($0.06AF_y$) due to uplift. The maximum moment observed at the base and top end of this column were $1.21R_yM_{px}$ and $0.30R_yM_{px}$, respectively. No noticeable strength deterioration or local buckling and very limited axial shortening with a maximum amplitude of 0.09%L were observed. Lower weak-axis bending with
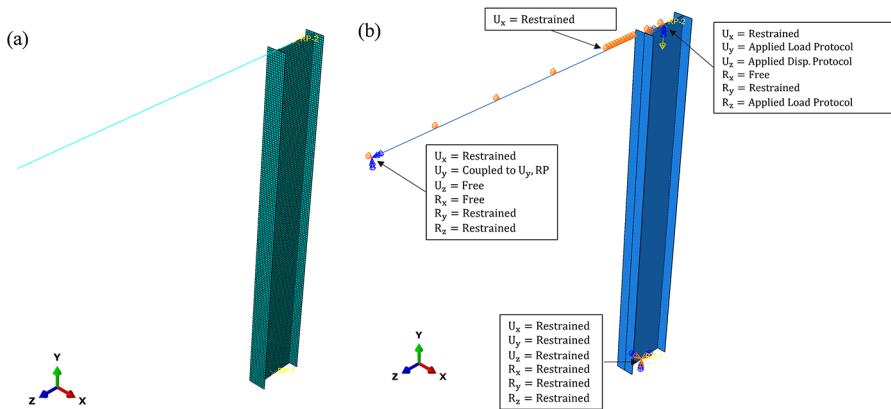
Fig. 7 Isolated interior first-storey column: (**a**) Finite element model; (**b**) Boundary conditions

the peak being $0.16R_yM_{py}$ at 3.4% drift ratio was induced in this column compared to that observed in the interior counterpart.

5 Evaluation of column stability parameters

The parameters affecting out-of-plane stability of wide-flange columns located in the first storey of Ductile steel MRFs were examined using the finite element model of an isolated first-storey column under a constant axial compression force, strong-axis (in-plane) displacement and weak-axis (out-of-plane) bending moment histories.

5.1 Component-based finite element model

The computationally-efficient numerical model of a wide-flange column isolated from the MRF was developed for the purpose of the numerical parametric study. Figure 7 shows the finite element model and the boundary conditions assigned. This model consisted of a wide-flange column constructed using shell elements (S4R) with a uniform mesh size of 25×25 mm and a wide-flange beam extending between the column top end and beam mid-span simulated using wire elements. The beam was intended to simulate the in-plane flexibility of the beam-to-column joint while representing flexural demands transferred from adjoining beams to the column at the joint. The material assigned to the column elements was identical to that described in Islam and Imanpour (2022). The elements simulating the RBS in the beam was defined using an elastic-perfectly plastic model with the probable yield strength of steel, however, an elastic material was used to simulate the rest of the beam outside of the RBS. At the column base, all DOFs were restrained. The translation and rotation of the column nodes at its top end were coupled to the reference point located at the middle of the column web (RP in Fig. 7b). The out-of-plane translational DOF of the RP was restrained, while the other two translational DOFs were controlled by the axial load and displacement history applied along Y- and Z-axes, respectively. The rotational DOF of the RP about X-axis was released since it is simulated explicitly using the first-storey beam. The
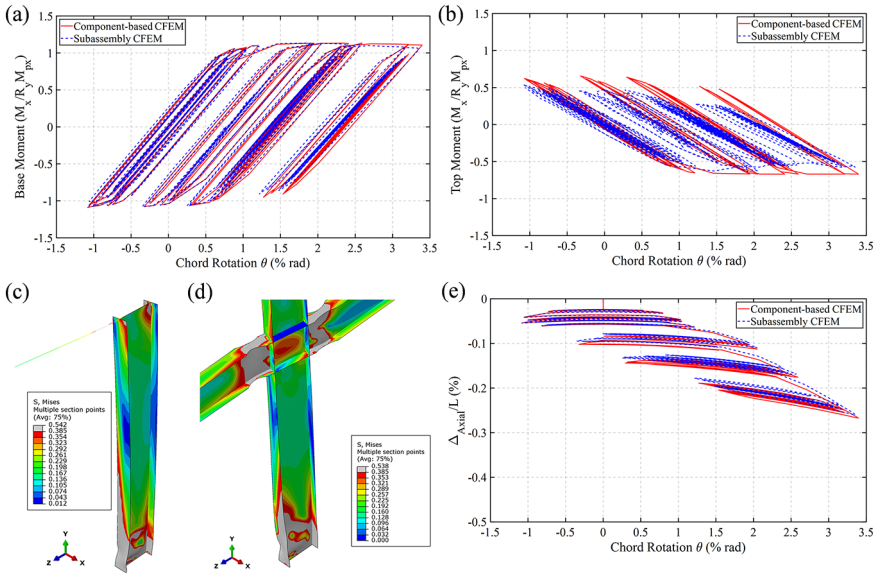
Fig. 8 Response of W610×153 column, component-based model versus subassembly model under the 2011 Tohoku, Japan – YMT002 earthquake: (**a**) Base in-plane moment; (**b**) Top in-plane moment; (**c-d**) Column deformed-shape and von Mises stress distribution from the component-based model and the subassembly model at t=156s, chord rotation 3.4% rad. (gray area represents yielding region); (**e**) Axial shortening

rotational DOF about Y-axis (twist) was fixed at the top end of the column to account for torsional and warping stiffness provided by upper-storey columns not modelled here. The rotational DOF about Z-axis was released to allow for the application of weak-axis bending moment history. The translational and rotational DOFs of the beam ends at the top end of the column were tied to those of the column to create a rigid connection. At the opposite end of the beam, the translation along X-axis and rotations about Y- and Z-axes were fixed, whereas the translation along Z-axis and rotation about X-axis were released. At the same end of the beam, the translation along Y-axis was coupled to the longitudinal displacement of the column's top end. The lateral out-of-plane movement of the beam was restrained in X-axis (Fig. 7b) as weak-axis bending produced by the beam out-of-plane response was directly imposed on the column. Other modeling assumptions followed those described in Islam and Imanpour (2022).

The modeling technique employed to construct the computationally-efficient component-based model of the isolated column was validated using three categories of metrics: (1) global response and damage modes, (2) end moments, and (3) axial shortening response under the 2011 Tohoku, Japan – YMT002 earthquake. For the verification purpose, the lateral strong-axis displacement, axial load, and weak-axis bending histories as obtained from the dynamic analysis of the MRF subassembly were applied at the top end of the isolated column model using a static analysis method. Figure 8a and b compare the moment responses at the base and top end of the column, respectively, predicted by the component-based model and those obtained from the NLRHA of the MRF subassembly model. Referring to Fig. 8a and b, the moments from both component-based and subassembly models
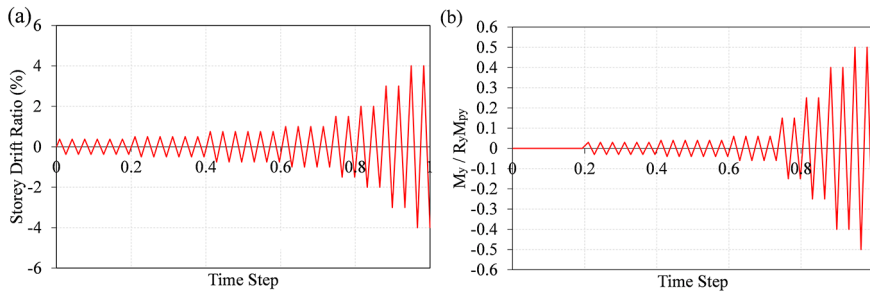
Fig. 9 Component-based finite element model loading scheme: (**a**) In-plane displacement history; (**b**) Weak-axis bending moment history

agreed well. Degradation of the top moment predicted by the subassembly model may be attributed to twisting of the column top end, which was not allowed in the component-based model. The column deformed shapes at $t=156s$, corresponding to a chord rotation of 3.4%, from the component-based and subassembly models are shown in Fig. 8c and d, respectively. A very good match was obtained between two models when predicting yielding regions, local bucking locations and amplitude, and distribution of von Mises stresses. The comparison of column axial shortening between two modeling approaches shown in Fig. 8e further confirmed the capability of the computationally-efficient component-based model to predict the cyclic response of fixed-base MRF columns.

5.2 Loading scheme

The cyclic loading protocol proposed by AISC Seismic Provisions (Fig. 9a) was used here to simulate the in-plane cyclic displacement anticipated under seismic loads. This protocol was preferred over the displacement history obtained from a ground motion record as it is expected to lead to more conservative in-plane demands on the column, thus providing an envelope of anticipated seismic demands, in particular, in the west coast of Canada that deep and long duration subduction earthquakes are expected (Suzuki and Lignos 2021). The maximum storey drift angle applied to the column was 4%, which can conservatively represent the NBC design-level hazard. The column was also subjected to a constant gravity-induced axial compression equal to $0.15AF_y$, representing an axial load level observed in typical Type D MRFs such as the one designed in this study. This compression load corresponds to 14% of the probable axial capacity (AR_yF_y) assumed in the model.

Weak-axis bending moment history shown in Fig. 9b was used to conservatively reproduce out-of-plane bending observed at the top end of the first storey MRF column under seismic ground motions (e.g., Fig. 6a). The weak-axis bending history represents the envelope of out-of-plane moments from the subassembly model NLRHA under the selected records. The weak-axis moment demand for the storey drift angles outside of the 3.4% storey drift ratio was extrapolated owing to the fact that first-storey column out-of-plane bending increases almost linearly as the column chord rotation increases.

Table 1 Geometrical properties and cross-section capacities of parametric study matrix

Section	L_b (m)	L_b/r_y	d/b_f	b/t_f	$(b/t_f)/$ $(b/t_f)_{Class 1}$	h/t_w	$(h/t_w)/$ $(h/t_w)_{Class 1}$	GJ/L (kN-m)	AR_yF_y (kN)	R_yM_{px} (kN-m)	R_yM_{py} (kN-m)
W360×237	4.3	42.2	0.96	6.56	0.84	17.0	0.31	146.7	11,589	1810	920
W360×237	6.3	61.8	0.96	6.56	0.84	17.0	0.31	100.1	11,589	1810	920
W530×150	3.3	45.0	1.74	7.68	0.99	39.6	0.72	50.6	7392	1598	389
W530×150	4.3	58.6	1.74	7.68	0.99	39.6	0.72	38.8	7392	1598	389
W530×150	5.3	72.2	1.74	7.68	0.99	39.6	0.72	31.5	7392	1598	389
W530×150	6.3	85.8	1.74	7.68	0.99	39.6	0.72	26.5	7392	1598	389
W530×182	3.3	44.5	1.75	6.45	0.83	33.0	0.60	87.2	8932	1937	477
W530×182	4.3	58.0	1.75	6.45	0.83	33.0	0.60	66.9	8932	1937	477
W530×182	5.3	71.4	1.75	6.45	0.83	33.0	0.60	54.3	8932	1937	477
W530×182	6.3	84.9	1.75	6.45	0.83	33.0	0.60	45.7	8932	1937	477
W610×125	3.3	66.7	2.67	5.84	0.75	48.1	0.87	35.9	6122	1413	206
W610×125	4.3	86.9	2.67	5.84	0.75	48.1	0.87	27.5	6122	1413	206
W610×125	5.3	107.1	2.67	5.84	0.75	48.1	0.87	22.4	6122	1413	206
W610×125	6.3	127.3	2.67	5.84	0.75	48.1	0.87	18.8	6122	1413	206
W610×153	3.3	65.3	2.72	4.60	0.59	40.9	0.74	68.5	7508	1767	262
W610×153	4.3	85.1	2.72	4.60	0.59	40.9	0.74	52.6	7508	1767	262
W610×153	5.3	105.0	2.72	4.60	0.59	40.9	0.74	42.7	7508	1767	262
W610×153	6.3	124.8	2.72	4.60	0.59	40.9	0.74	35.9	7508	1767	262
W610×174	3.3	44.2	1.90	7.52	0.96	41.0	0.74	65.3	8547	2064	450
W610×174	4.3	57.6	1.90	7.52	0.96	41.0	0.74	50.1	8547	2064	450
W610×174	5.3	71.0	1.90	7.52	0.96	41.0	0.74	40.6	8547	2064	450
W610×174	6.3	84.3	1.90	7.52	0.96	41.0	0.74	34.2	8547	2064	450
W610×217	3.3	43.1	1.91	5.92	0.76	34.6	0.63	130.1	10,665	2637	589
W610×217	4.3	56.2	1.91	5.92	0.76	34.6	0.63	99.8	10,665	2637	589
W610×217	5.3	69.3	1.91	5.92	0.76	34.6	0.63	81.0	10,665	2637	589
W610×217	6.3	82.4	1.91	5.92	0.76	34.6	0.63	68.1	10,665	2637	589

5.3 Parametric study matrix

An ensemble of 26 Class 1 steel wide-flange columns – that also meet the width-thickness ratio for highly compact members in AISC Seismic Provisions, except for W530×150 and W610×174 where the flange width-to-thickness ratio slightly exceeds the AISC limit – representing interior MRF columns was selected to evaluate column stability response. The selected sections, plus their geometric properties and cross-sectional capacities, are given in Table 1. In this table, the unbraced length L_b is the distance from the fixed base to the beam-to-column centerline. The parametric study matrix was selected such that while creating a wide range of column stability influential parameters, including the global slenderness ratio $42.2 \leq L_b/r_y \leq 127.3$, section aspect ratio $0.96 \leq d/b_f \leq 2.72$, flange width-to-thickness ratio $6.56 \leq b/t_f \leq 7.68$ ($0.59 \leq (b/t_f)/(b/t_f)_{Class1} \leq 0.99$), and web width-to-thickness ratio $17.0 \leq h/t_w \leq 48.1$ ($0.31 \leq (h/t_w)/(h/t_w)_{Class1} \leq 0.87$), they can represent practical and available profiles used in low-to-mid-rise steel MRF buildings in North America, with the emphasis on deep ($d/b_f \geq 1.7$) sections, which favor a more economical MRF design. Deep sections included W530×150, W530×182, W610×125, W610×153, W610×174 and W610×217 profiles. In addition to deep sections, a square ($d/b_f \approx 1.0$) W360×237 profile was chosen as

a baseline column. Four unbraced heights L_b = 3.3, 4.3, 5.3, and 6.3 m were considered for deep members, while the W360×237 column had L_b = 4.3 and 6.3 m. The selected heights cover potential first-storey columns in low-to-mid-rise steel MRF buildings for typical office, hotel, or residential occupation. For each wide-flange column in the parametric study matrix, a wide-flange beam was selected such that the inflection point in the elastic range is kept at a distance of approximately $0.75L_b$ measured from the column base. This is expected in typical first-storey MRF columns under lateral loading when the column remains elastic (Zareian et al. 2010). The beam connected to the top end of the column would allow the column to reach a maximum strong-axis moment of approximately $0.65R_yM_{px}$ at its top end once plastic hinging occurs at the RBS. This top moment would feature a moment diagram with an inflection point at 0.6 to 0.7 L measured from the column base in the elastic range, which was evidenced by previous studies (Elkady and Lignos 2018b).

5.4 Analysis results

The results obtained from the column stability parametric study were used to compute four strength and deformation response parameters that can be used to quantitatively assess the out-of-plane stability response of the columns and establish a set of criteria to identify column failure modes. These parameters included flexural strength at the base, axial shortening, cross-section twist, and out-of-plane displacements. Twist angles and out-of-plane displacements were recorded at quarter points along the length of the member measured from the column base, i.e., at 0.25 L, 0.50 and 0.75 L (see Fig. 6d). Table 2 summarizes these parameters for the 26 columns analyzed under the axial load of $0.15AF_y$. The peak response parameters were recorded at 4% storey drift ratios, except those that failed before the last cycle of the target drift was attained as shown in Table 2.

Two failure modes dominated the out-of-plane stability response of the columns that failed under cyclic loading: (1) out-of-plane buckling at the column base due to severe local buckling, and (2) member buckling along the length of the column. Both failure modes are accompanied by severe strength degradation leading to the loss of column load-carrying capacity. Figure 10a and b show an example of out-of-plane buckling at the base observed for the 4.3 m-long W610×153 column and an example of member buckling observed for the 5.3 m-long W610×153 column, respectively.

Column strength and deformation response parameters (reported in Table 2) are plotted against two geometric parameters, L_b/r_y and d/b_f, in Fig. 11. As shown, both stocky W360×237 columns exhibited no noticeable strength degradation owing to their stable cyclic response with minor web and flange local buckling at the base (Newell and Uang 2008), even in the presence of fairly considerable weak-axis bending. The results of deep columns showed severe strength degradation compared to R_yM_{px}. Referring to Fig. 11a, b and a descending trend was observed for the flexural strength of the column as both L_b/r_y and d/b_f increase. All three deformation parameters, axial shortening, out-of-plane displacement, and cross-section twist are plotted against L_b/r_y and d/b_f as shown in Fig. 11c to h. All three deformation parameters increase as either d/b_f or L_b/r_y increases, except axial shortening against L_b/r_y for which no clear trend was observed. In general, shorter columns, L_b = 3.3 and 4.3 m, that failed exhibited large axial shortening (>2%L) and out-of-plane displacement near the base plastic hinge (>2%L) accompanied by large strength deterioration, promoting column out-of-plane buckling at the base due to severe local buckling

Table 2 Measured response parameters for columns under an axial load of $0.15AF_y$.

Section	L_b (m)	Max. Achieved Drift (%)	M_{rx}/R_yM_{px}	Δ_{Axial}/L (%)	$\Delta_{out-of-plane}/L$ (%)	$\gamma_{cross-section}$ (% rad)	Failure Mode
W360×237	4.3	4.0	1.07	0.6	0.2	2.9	-
W360×237	6.3	4.0	1.13	0.3	0.3	5.3	-
W530×150	3.3	4.0	0.55	2.3	1.0	3.7	-
W530×150	4.3	4.0	0.64	1.6	0.5	2.6	-
W530×150	5.3	4.0	0.61	1.3	0.5	9.8	-
W530×150	6.3	4.0	0.50	1.2	0.9	10.5	-
W530×182	3.3	4.0	0.78	1.8	0.6	3.2	-
W530×182	4.3	4.0	0.83	1.3	0.3	2.9	-
W530×182	5.3	4.0	0.74	1.1	0.6	8.4	-
W530×182	6.3	4.0	0.67	1.0	0.8	10.4	-
W610×125	3.3	4.0	0.19	4.0	3.4	4.5	Out-of-plane buckling at base
W610×125	4.3	4.0	0.22	2.7	2.1	4.8	Out-of-plane buckling at base
W610×125	5.3	4.0	0.36	1.9	5.6	18.9	Member buckling
W610×125	6.3	3.0	0.46	0.9	4.2	13.3	Member buckling
W610×153	3.3	4.0	0.34	3.3	3.4	5.4	Out-of-plane buckling at base
W610×153	4.3	4.0	0.39	2.2	2.0	5.8	Out-of-plane buckling at base
W610×153	5.3	4.0	0.41	2.0	6.5	15.9	Member buckling
W610×153	6.3	3.0	0.46	1.2	5.3	17.2	Member buckling
W610×174	3.3	4.0	0.45	2.9	1.6	4.0	-
W610×174	4.3	4.0	0.51	2.1	0.9	3.5	-
W610×174	5.3	4.0	0.61	1.5	0.5	3.5	-
W610×174	6.3	4.0	0.46	1.4	1.1	11.7	Member buckling
W610×217	3.3	4.0	0.68	2.3	1.2	4.1	-
W610×217	4.3	4.0	0.74	1.7	0.6	3.6	-
W610×217	5.3	4.0	0.74	1.3	0.5	9.5	-
W610×217	6.3	4.0	0.62	1.2	1.0	11.1	-

near the plastic hinge location. Whereas longer, 5.3 and 6.3 m columns underwent a large cross-section twist angle (>0.10 rad.) near the base plastic hinge plus large out-of-plane deformations propagated over the member height; this was accompanied by large strength deterioration, suggesting a tendency for member buckling.

A set of strength and deformation criteria was established to identify whether a column has failed. These criteria are (1) flexural strength falling below 50% times the member's probable plastic moment capacity R_yM_{px} accompanied by axial shortening and out-of-plane displacement measured near the base plastic hinge exceeding 2%L, which represents out-of-plane buckling at the base, and (2) flexural strength lower than $0.50R_yM_{px}$ accompanied by a cross-section twist angle greater than 0.08 rad., which represents member buckling. Both failure modes were intended to characterize a condition in which the column experiences the complete loss of gravity load-carrying capacity i.e., dynamic instability. The respective failure mode for the columns that experienced instability is given in Table 2. All W610×125

(a)

(b)
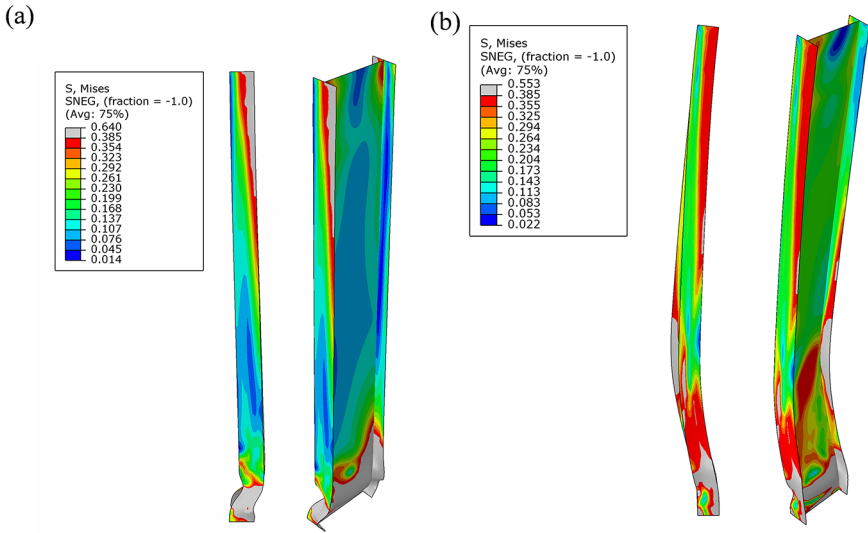
Fig. 10 In-plane and out-of-plane deformed-shape and von Mises stress distribution at the end of the analysis of columns under an axial load of $0.15AF_y$: (**a**) W610×153 column with $L_b/r_y = 85.1$, $d/b_f = 2.72$, $h/t_w = 40.9$ - out-of-plane buckling at the base; (**b**) W610×153 column with $L_b/r_y = 108$, $d/b_f = 2.72$, $h/t_w = 40.9$ - member buckling

and W610×153 columns failed. For 3.3 m- and 4.3 m-long members, failure was dominated by out-of-plane buckling at the base due to out-of-plane displacements exceeding $2\%L$ accompanied by considerable axial shortening. However, the 5.3 m- and 6.3 m-long columns failed due to member buckling accompanied by twist angles well above 0.08 rad. Note that the 6.3 m-long W610×125 and W610×153 columns failed to reach 4% drift ratios. In addition to W610×125 and W610×153 columns, only the 6.3 m-long W610×174 column failed in the member buckling mode experiencing a twist angle exceeding 0.11 rad. No buckling was observed for the rest of the columns studied here. The failure cases are shown in Fig. 11 using a hollow marker. As shown, the cases identified as "Buckled" almost always lie on the boundary of L_b/r_y and d/b_f axes, i.e., $L_b/r_y > 65$ and $d/b_f > 2.6$, suggesting the correlation between the column stability condition and global slenderness and cross-section aspect ratios. Furthermore, columns with a higher d/b_f remained stable only when L_b/r_y is low and those with high L_b/r_y require sections with $d/b_f \approx 1.0$ to avoid instability.

The column parametric study was repeated under a higher axial load of $0.25AF_y$, which corresponds to 23% of the probable axial capacity (AR_yF_y) of the column. The measured response parameters for the 26 columns analyzed under the axial load of $0.25AF_y$ are summarized in Table 3. Under this higher axial load level, the W360×237 columns still exhibited a stable behaviour with limited strength degradation. The deep columns, however, exhibited severe strength degradation exceeding $0.60R_yM_{px}$, high axial shortening (on average $3\%L$), and out-of-plane displacement (on average $2.6\%L$). The shorter 3.3 m- and 4.3 m-long columns experienced out-of-plane buckling at the base due to severe out-of-plane displacements near the base plastic hinge (close to or exceeding $2.0\%L$) accompanied by large axial shortening ($>2\%L$). Columns with a length equal to 5.3 or 6.3 m failed by member buckling and experienced large twist (on average 0.14 rad.). In particular, 5.3 m-
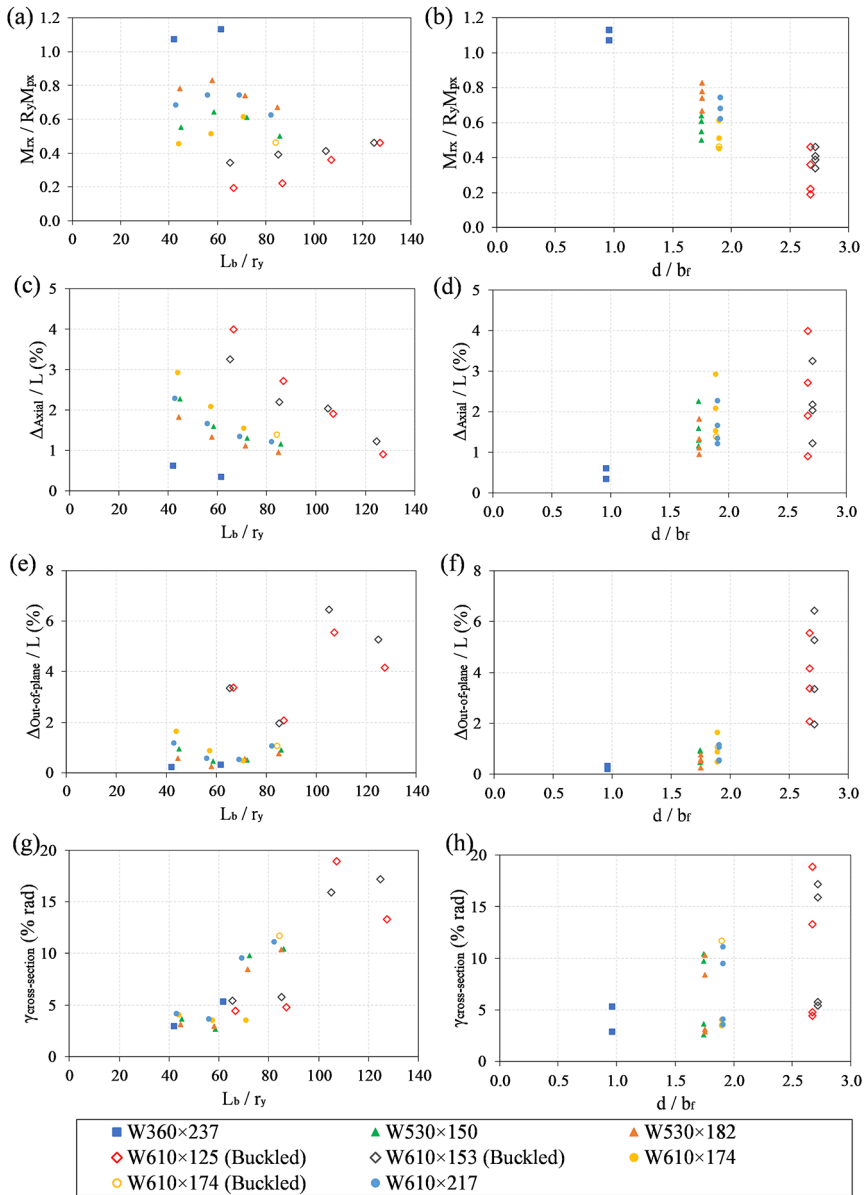
Fig. 11 Column strength and deformation response parameters under an axial load of $0.15AF_y$: (**a-b**) Flexural strength at the base vs. L_b/r_y and d/b_f; (**c-d**) Axial shortening vs. L_b/r_y and d/b_f; (**e-f**) Out-of-plane displacement at the base vs. L_b/r_y and d/b_f; (**g-h**) Cross-section twist angle vs. L_b/r_y and d/b_f (data points with a hollow marker indicate failure)

Table 3 Measured response parameters for columns under an axial load of $0.25AF_y$.

Section	L_b (mm)	Max Achieved Drift (%)	M_{rx}/R_yM_{px}	Δ_{Axial}/L (%)	$\Delta_{out-of-plane}/L$ (%)	$\gamma_{cross-section}$ (% rad)	Failure Type
W360×237	4300	4.0	0.90	1.1	0.2	3.5	-
W360×237	6300	4.0	0.95	0.6	0.4	8.5	-
W530×150	3300	4.0	0.05	5.3	3.0	3.9	Out-of-plane buckling at base
W530×150	4300	4.0	0.12	3.5	1.8	4.1	Out-of-plane buckling at base
W530×150	5300	4.0	0.20	2.6	2.4	9.5	Member buckling
W530×150	6300	4.0	0.17	2.3	2.8	9.0	Member buckling
W530×182	3300	4.0	0.29	3.9	2.2	4.1	Out-of-plane buckling at base
W530×182	4300	4.0	0.40	2.7	1.1	5.1	Out-of-plane buckling at base
W530×182	5300	4.0	0.32	2.3	1.9	10.4	Member buckling
W530×182	6300	4.0	0.32	1.9	1.9	11.4	Member buckling
W610×125	3300	3.0	0.08	4.0	3.7	3.5	Out-of-plane buckling at base
W610×125	4300	3.0	0.09	3.2	2.9	4.6	Out-of-plane buckling at base
W610×125	5300	2.0	0.45	0.9	3.2	15.3	Member buckling
W610×125	6300	2.0	0.57	0.5	3.1	10.7	Member buckling
W610×153	3300	4.0	0.07	5.4	5.3	4.6	Out-of-plane buckling at base
W610×153	4300	3.0	0.18	2.8	2.9	4.7	Out-of-plane buckling at base
W610×153	5300	2.0	0.42	1.0	3.9	12.8	Member buckling
W610×153	6300	2.0	0.58	0.5	3.1	8.5	Member buckling
W610×174	3300	4.0	0.11	5.4	3.3	3.4	Out-of-plane buckling at base
W610×174	4300	4.0	0.03	4.3	2.6	3.6	Out-of-plane buckling at base
W610×174	5300	4.0	0.16	3.4	0.8	31.4	Member buckling
W610×174	6300	4.0	0.20	2.2	2.5	8.2	Member buckling
W610×217	3300	4.0	0.20	5.0	3.3	4.3	Out-of-plane buckling at base
W610×217	4300	4.0	0.23	3.6	2.1	4.5	Out-of-plane buckling at base
W610×217	5300	4.0	0.26	2.7	1.0	29.2	Member buckling
W610×217	6300	4.0	0.26	2.3	2.6	10.7	Member buckling

and 6.3 m-long W610×125 and W610×153 columns failed to reach 3.0% drift cycles. The majority of the columns showing member buckling also experienced appreciable axial shortening (on average 1.9%L) and out-of-plane displacement at the bottom half of the member (on average 2.4%L). The correlations between the column strength and deformation response parameters and the column failure modes observed under an axial load equal to $0.25AF_y$ agree with those described under an axial load of $0.15AF_y$ (Fig. 11). Moreover, the results under the heavier axial load confirmed the detrimental impact of the axial load
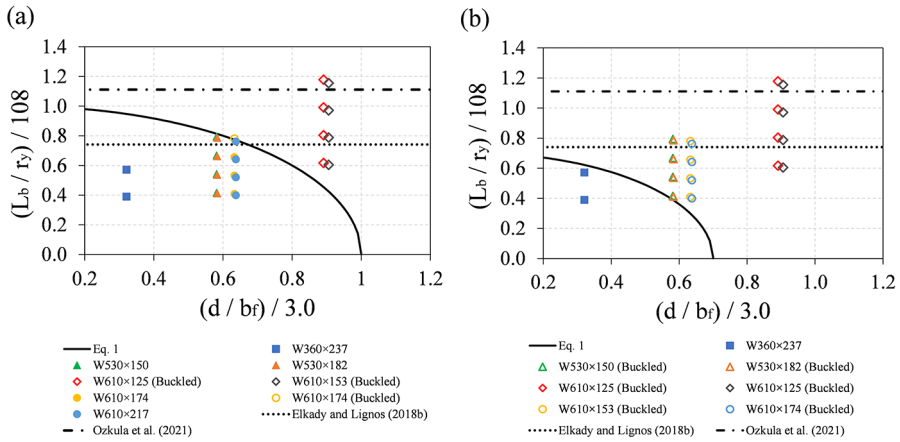
Fig. 12 Proposed stability design equation: (**a**) $0.15AF_y$ axial load level; (**b**) $0.25AF_y$ axial load level (data points with an empty marker indicate failure)

level on the column cyclic response (Elkady and Lignos 2018b; Ozkula et al. 2017a, 2021), which shall be considered when checking column stability under seismic loads.

5.5 Stability design recommendations

On the basis of the column stability parametric study presented herein, in particular, the correlation between the column strength and deformation response parameters and the geometrical properties, including the member global slenderness ratio L_b/r_y and cross-section aspect ratio d/b_f, and the axial load ratio, an empirical equation for evaluating the out-of-plane stability of wide-flange MRF columns with base plastic hinging was developed as follows:

$$\left(\frac{C_f/AF_y}{0.15}\right)^{1.4}\left[\left(\frac{L_b/r_y}{108}\right)^2 + \left(\frac{d/b_f}{3.0}\right)^2\right] \leq 1.0 \tag{1}$$

The proposed equation couples the global slenderness ratio, cross-section aspect ratio, which can indirectly represent web width-to-thickness ratio for Class 1 sections (or highly compact sections in AISC Seismic Provisions), and axial load ratio to predict the stability condition of wide-flange columns with base plastic hinging. The proposed stability design equation is given in Fig. 12a and b against the column cases that failed and passed the criteria described earlier under $0.15AF_y$ and $0.25AF_y$ axial load levels, respectively. As shown, the proposed equation can well predict the adequacy of columns with $d/b_f \approx 1.0$ while eliminating deep slender columns with $d/b_f > 2.6$ such as the W610×125 or W610×153 sections under the $0.15AF_y$ axial load level (Fig. 12a) and all deep columns, i.e., $d/b_f > 1.75$, under the $0.25AF_y$ axial load level (Fig. 12b). Furthermore, the range of acceptable section aspect ratios in this equation, i.e., $d/b_f = 0.0$ to 3.0, encompasses the majority of Class 1 wide-flange profiles that would be used in practice as first-storey columns in low and mid-rise steel MRF build-

ings. The results presented in Fig. 12 confirms that the proposed stability design equation can efficiently represent the stability condition of wide-flange columns while offering a more inclusive design check compared to a set of uncoupled checks currently specified in CSA S16. The stability design equation is also compared in Fig. 12 with the constant limiting ratios proposed in the past, namely the global slenderness limit of $L_b/r_y = 80$ proposed by Elkady and Lignos (2018b) for the Canadian design practice and the global slenderness limit of $L_b/r_y = 120$ proposed by Ozkula et al. (2021) in the framework of AISC Seismic Provisions. As shown in Fig. 12, the proposed equation here can be used as an alternative approach to check out-of-plane stability of MRF columns with base plastic hinging taking into account the combined effect of the column axial load, member slenderness, and cross-section aspect ratios.

6 Limitations

Although the current study offered an improved understanding of the seismic stability of wide-flange columns located in the first storey of Ductile steel MRFs and proposed design recommendations for out-of-plane stability of such columns, which appears to properly represent the stability condition of these columns while improving the current design requirements (e.g., uncoupled requirements implicit in the current Canadian steel design standard), an examination of the limitations of the study is critical.

The findings of this study should be used within the range of geometrical and constitutional parameters considered here. The current study is limited to steel MRFs part of a mid-rise office building located in high seismic region of Canada. Given that the number of stories, number of MRF bays, soil type and seismic hazard would affect the seismic-induced demands on first-storey MRF columns, future studies should consider taller prototype buildings provided that wide-flange sections are still practical for their MRF columns, MRFs with smaller and larger number of bays compared to 5-bay MRF studied here, MRFs located in moderate seismic regions, and those subjected to other seismic hazard sources.

A note of caution here is that the results of NLRHA presented here are based on a set of ground motion records scaled to match the 2015 NBC design level earthquake spectrum, which is representative of a 2% probability of being exceeded in 50 years. Future studies should also examine the collapse performance of such frames. Moreover, the MRF subassembly model was analyzed under three (most critical) ground motions due to the high computational cost of the detailed finite element model under dynamic loading.

The examination of the stability response of MRFs in this study was limited to a 2D frame and the out-of-plane frame motion that would occur in a 3D building, which would contribute to the out-of-plane response of MRF columns, was not studied here. Such three-dimensional response should be investigated in future studies and its effects on the stability design of wide-flange columns should be quantified.

Future experimental studies should further validate the findings of this study using laboratory testing of isolated wide-flange columns or hybrid simulation of steel MRFs. Future studies should also explore the possibility of adapting traditional axial force-bending moment interaction equations developed based on mechanics and stability principles to verify the stability of beam-columns with base plastic hinging, e.g., fixed-based MRF columns (Imanpour et al. 2016).

7 Conclusion

This paper assessed the stability response of wide-flange columns located in the first storey of Ductile steel MRFs under seismic loads with emphasis on their out-of-plane stability and proposed enhanced stability design recommendations. A prototype steel MRF consisting of deep column sections ($d/b_f \approx 2.7 > 1.7$) was first designed per the Canadian steel design standard. The three-dimensional continuum-based finite element model (CFEM) of the MRF subassembly consisting of the exterior bay plus half of the adjacent interior bay was then developed. The MRF subassembly was analyzed under earthquake ground motions to evaluate the stability response of its first-storey columns. The MRF subassembly was also used to verify the suitability of a component-based column model, which is isolated from the MRF, in predicting column nonlinear cyclic response. The corroborated isolated column model was used to examine the stability response of a set of 26 wide-flange columns by varying L_b/r_y, d/b_f, b/t_f, h/t_w and C_f/AF_y under a constant axial compression load, strong-axis cyclic displacement and weak-axis flexural bending histories. The results of the column parametric study were finally used to propose design recommendations for out-of-plane stability of wide-flange columns. The key findings of this study are summarized as follows:

- The out-of-plane displacement and twist of the interior first-storey column triggered by RBS out-of-plane movement is amplified at large storey drifts by local buckling near the column base. Weak-axis flexural bending of the column reached $0.40R_yM_{py}$ at 3.4% drift.
- Lesser out-of-plane displacements, twist and weak-axis bending were observed for the exterior first-storey column compared to those recorded for the interior first-storey column, which was mainly attributed to the fact that these columns benefit from overturning effects leading to highly fluctuating axial loads. This suggests that the CSA S16 limit on the axial load, i.e., $0.30AF_y$, may be conservative for exterior columns of Ductile MRFs.
- Four strength and deformation response parameters, including flexural strength, axial shortening, cross-section twist and out-of-plane displacements, were identified for columns based on a parametric study database to quantitatively assess their stability response and establish a set of criteria to identify column failure modes.
- The parametric study of 26 Class 1 wide-flange columns showed that two failure modes dominate the stability response of deep ($d/b_f \geq 1.7$) wide-flange columns: (1) out-of-plane buckling at the column base associated with severe local buckling observed in shorter columns ($L \leq 4.3$ m) and characterized by axial shortening and out-of-plane displacement near the base greater than $2\%L$; (2) member buckling associated with lateral out-of-plane deformation over the column length recorded for longer columns ($L \geq 5.3$ m) and characterized by a large cross-section twist angle exceeding 0.08 rad. Both failure modes were accompanied by severe strength degradation resulting in flexural strength falling below 50% of the plastic moment capacity, i.e., $0.50R_yM_{px}$.
- Under the $0.15AF_y$ axial load level, all W610×125 and W610×153 columns failed due to significant strength degradation plus excessive shortening and twist at 4% drift ratio. The 3.3 and 4.3 m-long W610×125 and W610×153 columns failed by out-of-plane buckling at the base, while the longer 5.3 and 6.3 m columns failed due to member

buckling. The 6.3 m-long W610×174 column failed by member buckling. No buckling was observed for other columns.

- The heavier axial load $0.25AF_y$ imposed on the parametric study columns resulted in more severe local bucking near the base and accelerated flexural strength degradation compared to columns under an axial load of $0.15AF_y$. All deep columns failed under the higher axial load level. Similar correlations to those identified for columns with the $0.15AF_y$ axial load were found between the column strength and deformation response parameters and failure modes.

- The results of the column stability parametric study confirmed a descending trend for the flexural strength of the column as both L_b/r_y and d/b_f increase. All three deformation response parameters, axial shortening, out-of-plane displacement, and cross-section twist, increase by increasing L_b/r_y and d/b_f, except axial shortening against L_b/r_y.

- An equation that couples the global slenderness, cross-section aspect ratio and axial load ratio was developed to predict the out-of-plane stability condition of wide-flange columns with base plastic hinging. This equation offers a more representative and inclusive stability design check than a set of uncoupled lateral bracing and axial force ratio checks currently prescribed by CSA S16.

Data Availability Not applicable.

Code Availability Not applicable.

Declarations

Conflicts of Interest The authors declare they have no relevant financial or non-financial interests to disclose.

Ethics approval Not applicable.

Consent to participate Not applicable.

Consent for publication Not applicable.

References

AISC (2016a) *Seismic provisions for structural steel buildings*. ANSI/AISC 341 – 16. American Institute of Steel Construction

AISC (2016b) *Code of standard practice for steel buildings and bridges*. ANSI/AISC 303 – 16. American Institute of Steel Construction

AISC (2016c) Prequalified for special and intermediate steel moment frames for seismic applications, ANSI/AISC 358 – 16. American Institute of Steel Construction, In. Chicago, IL, USA

ASTM (2003) *Standard specification for general requirements for rolled structural steel bars, plates, shapes, and sheet piling*, ASTM A6/A6M-04b. American Society for Testing and Materials

Brownlee SA (1994) *Axial force and plate slenderness Effects on the Inelastic Behaviour of Structural Steel Beam-Columns*. the University of Canterbury, Christchurch, New Zealand

CEN (2003) *Eurocode 8 – design provisions for earthquake resistant structures*, EN-1998-1:2003. E, Comite Europeen de Normalization, Brussels, Belgium

CSA (2019) *Design of steel structures*. Canadian Standards Association Group. Mississauga, ON, Canada

Chi B, Uang C-M (2002) Cyclic response and design recommendations of reduced beam section moment connections with deep columns. *J Struct Eng* 128(4):464–473

CISC (2014) *Moment Connections for Seismic Applications*, 2nd Edition. Canadian Institute of Steel Construction. Markham, ON, Canada

CISC (2021) *Handbook of steel construction*. Canadian Institute of Steel Construction. Markham, ON, Canada

Cravero J, Ahmed E, Lignos D (2020) Experimental evaluation and numerical modeling of wide-flange steel columns subjected to constant and variable axial load coupled with lateral drift demands. *J Struct Eng* 146(3):04019222

Dassault Systemes Simulia Corporation (2020)ABAQUS-FEA/CAE. In. RI, USA

de Castro e Sousa A, Suzuki Y, Lignos DG (2020) Consistency in solving the Inverse Problem of the Voce-Chaboche constitutive model for Plastic Straining. J Struct Eng 146(9):04020097

Elkady A, Lignos D (2014) Modeling of the composite action in fully restrained beam-to-column connections: implications in the seismic design and collapse capacity of steel special moment frames. *Earthq Eng Struct Dynamics* 43(13):1935–1954

Elkady A, Lignos D (2017) Stability requirements of deep steel wide-flange columns under cyclic loading. *Proceedings of the Annual Stability Conference Structural Stability Research Council*, San Antonio, Texas, USA

Elkady A, Lignos DG (2018a) Full-scale testing of deep wide-flange steel columns under multi axis cyclic loading: loading sequence, boundary effects, and lateral stability bracing force demands. *J Struct Eng* 144(2):04017189

Elkady A, Lignos DG (2018b) Improved seismic design and nonlinear modeling recommendations for wide-flange steel columns. *J Struct Eng* 144(9):04018162

FEMA (2000) *State of the art report on connection performance*, FEMA-355D. Federal Emergency Management Agency

Hartloper AR, de Castro Sousa A, Lignos DG (2021) Constitutive modeling of Structural Steels: nonlinear Isotropic/Kinematic hardening material model and its calibration. *J Struct Eng* 147(4):04021031

Imanpour A, Lignos D, Clifton C, Tremblay R (2016) Comparison of seismic design requirements for steel moment resisting frames with emphasis on stability of columns in North America, New Zealand, and Europe. *11th Pacific Structural Steel Conference*, Shanghai, China

Islam A, Imanpour A (2022) Stability of wide-flange columns in steel moment-resisting frames: evaluation of the canadian seismic design requirements. *Bulletien Earthq Eng* 20:1591–1617

Islam A (2022) *Improved seismic design recommendations for wide-flange columns in ductile steel moment-resisting frames considering three-dimensional response*. Department of Civil and Environmental Engineering, University of Alberta, Canada

MacRae GA, Carr AJ, Walpole WR (1990) *The seismic response of steel frames*, Report 90 – 6. University of Canterbury Research, University of Canterbury, Christchurch, New Zealand

McKenna F, Fenves GL, Scott MH (1997) Open System for Earthquake Engineering Simulation (OpenSees). In. University of California, Berkeley

Mokhtari M, Islam A, Imanpour A (2022) Development, seismic performance and collapse evaluation of steel 616 moment-resisting knee braced frame. *J Constr Steel Res* 197:107262

Nakashima M, Takanashi K, Kato H (1990) Test of steel beam-columns subject to sidesway. *J Struct Eng* 116(9):2516–2531

Newell JD, Uang C-M (2008) Cyclic behavior of steel wide-flange columns subjected to large drift. *J Struct Eng* 134(8):1334–1342

NRC (2015) National Building Code of Canada 2015. National Research Council of Canada

NRC (2015) User's guide – NBC 2015 structural commentaries (part 4 of Division B). Associate Committee on the National Building Code, Ottawa, ON

NZS (1997) *Steel structures standard*, NZS 3404: Part 1:1997. Standards New Zealand, Wellington, New Zealand

Ozkula G, Harris J, Uang C-M (2017a) Observations from cyclic tests on deep, wide-flange beam-columns. *Eng J Am Inst Steel Constr* 54:45–60

Ozkula G, Harris J, Uang C-M (2017b) Classifying cyclic buckling modes of steel wide-flange columns under cyclic loading. *ASCE Structures Congress*, Denver, CO, pp. 155–167

Ozkula G, Harris J, Uang C-M (2017c) Cyclic backbone curves for steel wide-flange columns: a numerical study. *Ce/Papers* 1(2–3):3365–3374

Ozkula G, Uang C-M, Harris J (2021) Development of enhanced seismic compactness requirements for webs in wide-flange steel columns. *J Struct Eng* 147(7):04021100

Penga BHH, MacRae GA, Walpole WR, Moss P, Dhakal RP, Clifton C, Hyland C (2008) Location of plastic hinges in axially loaded steel members. *J Constr Steel Res* 64:344–3516

Popov EP, Bertero VV, Chandramouli S University of California, B. E. E. R. C. (1975). *Hysteretic behavior of steel columns.*Earthquake Engineering Research Center, University of California, CA, USA

Popov EP, Yang T-S, Chang S-P (1998) Design of steel MRF connections before and after 1994 northridge earthquake. *Eng Struct* 20(12):1030–1038

Ricles JM, Zhang X, Lu L-W, Fisher JW (2004) *Development of seismic guidelines for deep column steel moment connections*. AISC/ATLSS Report No, Lehigh Univ., Bethlehem, PA, pp 04–13

Shen J, Associate S, Astaneh-Asl A, McCallen D (2002) *Use of deep columns in special steel moment frames*. Steel Tips, Structural Steel Educational Council

Suzuki Y, Lignos DG (2021) Experimental evaluation of steel columns under seismic hazard-consistent collapse loading protocols. *J Struct Eng* 147(4):04021020

Tremblay R, Atkinson GM, Bouaanani N, Daneshvar P, Leger P, Koboevic S (2015) Selection and scaling of ground motion time histories for seismic analysis using NBCC 2015. *The 11th Canadian Conference on Earthquake Engineering*, Victoria, BC, CA

Uang C-M, Ozkula G, Chansuk P (2019) Research on seismic design of deep wide-flange steel columns in the U.S. *12th Pacific Structural Steel Conference*, Tokyo, Japan, Tokyo, Japan

Yu QS, Gilton C, Uang CM, Sac JV (2001) *Cyclic response of RBS moment connections: Loading sequence and lateral bracing effects*, Rep. No. SSRP-99/13. Dept. of Structural Engineering, Univ. of California, San Diego, CA

Zhang X, Ricles JM (2006) Experimental evaluation of reduced beam section connections to deep columns. *J Struct Eng* 132(3):346–357

Zareian F, Lignos DG, Krawinkler H (2010) Evaluation of seismic collapse performance of steel special moment resisting frames using FEMA P695 (ATC-63) methodology. *ASCE Structures Congress*, Orlando, FL, May 12–15, pp 1275–1286

Authors and Affiliations

Abrar Islam[1] · Ali Imanpour[2]

✉ Ali Imanpour
imanpour@ualberta.ca

Abrar Islam
aislam1@ualberta.ca

[1] Graduate research assistant, Department of Civil and Environmental Engineering, University of Alberta, T6G 1H9 Edmonton, Canada

[2] Department of Civil and Environmental Engineering, University of Alberta, T6G 1H9 Edmonton, Canada